Synthesis of Tio_2 impregnated Ribes nigrum stem nanoactivated carbon and Their application to Remove Heavy Metals

Abstract

Nanoactivated carbons from *Ribes nigrum* (black currant) stem were prepared using two-step procedure with excellent yield and were characterized using different spectroscopic techniques. The FTIR spectroscopy revealed O-H, C=C, C=N, and C-O stretching. XRD analysis revealed the particle sizes as 29.57 nm for stem activated carbon (SAC) and 26.55 nm for stem activated carbon impregnated with titanium (SAT)while, the morphology of the SAC and SAT were revealed by SEM to be spherical, granular and porous. The prepared nanoactivated materials were used for the removal of Pb^{2+} and Cd^{2+} from aqueous solution. The influences of initial metal ion concentration, agitation time, adsorbent dose, temperature and pH were studied in batch experiments at room temperature. The adsorption equilibriums were rapid at 60 min of agitation for Pb^{2+} and Cd^{2+} on SAT with appreciable %removal. The adsorption data for Pb^{2+} and Cd^{2+} on SAT fitted well into Freundlich isotherm than Langmuir given correlation coefficient (R^2) very close to unity and appreciable maximum adsorption capacity K_F> 1.00. The fitting into Freundlich indicates multilayer coverage on the adsorbents. The kinetic studies showed good correlation coefficient for a pseudo-second order kinetic model for the SAT. The enthalpies of the adsorption process are: +12.754 and +18.377KJ mol^{-1} for Pb^{2+} and Cd^{2+}on SAT respectively. The entropies of the adsorption process were also evaluated and have been found to be +41.805 and +12.151 KJ mol^{-1} for Pb^{2+} and Cd^{2+}on SAT. The results showed that SAT has the potential to be applied as alternative low-cost nanoadsorbents in the remediation of metal contamination in water.

Keywords: nanoadsorbents, XRD analysis, heavy metals, carcinogens

Introduction

The direct or indirect discharge of heavy metals into aquatic systems has become a matter of concern in the world over the last few decades. They have been prioritized as major inorganic contaminants in the environment because of their accumulation tendency, hazardous effect, and toxicity to the human life and environmental health (Ahmed *et al.,* 2012). Heavy metals posed environmental pollution and have toxic effects on humans which are unfavorable to ecological, evolutionary, nutritional and environmental balances. These heavy metals are discharged into the environment through anthropogenic processes. In waste water, commonly found heavy metals include cadmium (Cd), arsenic (As), chromium (Cr), lead, copper (Cu), zinc (Zn) and nickel (Ni), all of these are causing risks to human health and the environmental balance by entering the surroundings via natural means and through human activities (Pindiga*et al.,* 2022).Their multiple industrial, domestic, agricultural, medical and technological applications have led to their wide distribution in the environment; raising concerns over their potential effects on human health and the environment. These metallic elements are considered systemic toxicants that are known to induce multiple organ damage, even at lower levels of exposure. They are also classified as human carcinogens according to the U.S. Environmental Protection Agency, and the International Agency for Research on Cancer.

Conventional methods of removing heavy metals from waste water, including chemical precipitation,

electro dialysis, ultrafiltration, ion exchange, membrane separation, chemical oxidation, coagulation, and flocculation. Some of these methods have been shown to be effective, however they have some limitations such as excess amount of chemical usage, accumulation of concentrated sludge that has serious disposal problems, formation of toxic compounds during the process, high cost, and incomplete removal of certain ions and takes long time for heavy metal removal. The major advantages of adsorption over these conventional treatment methods are low cost, high efficiency, minimization of chemicals, no additional nutrient requirement, and reuse of adsorbent for further metal uptake and possibility of metal recovery (Joshi, 2018).

Adsorption is a surface phenomenon in which the solutes are concentrated at the surface of adsorbent, and effective adsorbents which have a highly porous composition so that their surface area to volume ratio is very high. The solute particles are held in contact with the adsorbent by a combination of physical, ionic and chemical forces (Baskaralingam*et al.,* 2006).

Activated carbon is a solid, porous and black carbonaceous material that has an essentially graphitic structure. AC contain physical characteristic such as large internal surface area and pore volume. The increased interest in the use of agriculturally based precursors for the preparation of AC is partly due to its low cost, renewable source and it is a way of recycling agricultural wastes which could otherwise constitute environmental pollution, particularly as it relates to solid waste management (Abdul-Salam and Magaji, 2014). AC are widely used as an effective adsorbent for removal of heavy metals from waste water.

The black currant (*Ribes nigrum L., Grossulariceae*), is a small, perennial shrub native to central Europe, northern Asia and the United States including Nigeria. In addition to its anecdotal use in traditional herbal medicine, modern laboratories have demonstrated the potent anti-inflammatory, antioxidant and antimicrobial effects of black currant constituents on a myriad of disease states.The focus of this research was to explore the feasibility of black currant activated carbon for the removal of Pb^{2+} and Cd^{2+} ions from aqueous solutions and also to optimize the adsorption conditions that will ensure high Pb^{2+} and Cd^{2+} uptake.

Experimental

Sample collection and pre-treatment

The stem samples were collected within the Gombe State University Campus, Gombe, Nigeria.Theywere washed with tap water and rinsed with distilled water to remove all impurities, sun-dried for 2-days and transferred to oven for proper drying. All chemicals used in this study were of analytical grade. Working standard solutions were prepared from analytical grade reagents and by serial dilution from the stock solutions.

Production of Activated Carbon

A single and double step production was adopted where by carbonization and activation by thermal decomposition of the raw material already impregnated with activating agent was carried out. A 150 g

of the raw dried stem was soaked in 250 ml of 50% (v/v) H_3PO_4 acid at room temperature for 24 hr, the H_3PO_4 was decanted and the activated sample was washed thoroughly with deionized water until the pH reading was basic (7.6). The activated dried sample was carbonized in a muffle furnace at 400 °C for 90 min. After cooling, the carbonized material was weighed to determine percentage yield then divided into two portion equally. The first portion was pulverized to reduce the size and labelled as stem activated carbon (SAC). The second portion 50 g was soaked in an aqueous TiO_2 (4 g/100 ml of distilled water) and stirred for 6 hr at 35 °C temperature. The above procedure was repeated and percentage yield was also determined, recorded and labelled as stem activated carbon impregnated with titanium (SAT). The two AC samples were sieved using a 140 µm sieve. Thereafter, the sizes of the two samples were obtained from the XRD analysis and SAT was chosen because of its size for the experiments.

Characterization

The SAC and SAT efficiency were determined by mass difference between the starting raw stem and ACs obtained (Fapetu, 2000). The SAC and SAT moisture content were determined by oven drying at 103 °C (Hesse, 1997). The surface functional groups by Perkin Elmer spectrum model 10.0309. The ACs morphology was determined by SEM (Phenom world) while, the SAC and SAT crystalline sizes were determined by XRD. Using Debye Scherer equation which is given as below:

$$D = K\lambda/\beta\cos\Theta \quad (1)$$

where

D = Particles size = 0.94, K= Constant volume, λ = X-ray wavelength (0.154 nm), P = Line broadening at half the maximum intensity, θ = Braggs angle (in degree).

Batch Adsorption Experiment(29.57nm and 26.55nm)

For the batch adsorption studies, SAT was chosen because of it particle size (26. 55 nm) as compared to SAC (29.57 nm). The studies were conducted by investigating the effect of adsorbent dose, initial metal ion concentration, agitation time, pH and temperature. For adsorbent dose, 50 ml of the metal ions (Pb^{2+} and Cd^{2+}) were poured into five different beakers and then 0.1, 0.2, 0.3, 0.4, and 0.5 g of SAT were added t to each beaker respectively. The content was stirred for 30 min at room temperature and then filtered. The filtrate was then analyzed using AAS to determine the absorbance. The same procedure was followed for other effects. 1M HCl and 1 M NaOH were for pH adjustment. The amount of the metal ion adsorbed (q_e) on the SAT and the percentage removal of the metal ion were calculated as:

$$q_e = \frac{(C_0 - C_e)V}{W} \quad (2)$$

$$\%\ Removal = \frac{C_0 - C_e}{C_0} \times 100 \quad (3)$$

where; C_0 and C_e are the initial and equilibrium concentration (mg/L) respectively, V is the volume of the solution (L) and w is the amount of adsorbent (g).

Results and Discussion

The Table 1 summarized some of the characteristics of the ACs produced from black current stem (SAC and SAT). The Table 1 showed that the ACs produced has a good efficiency, moisture content when compared to results of other researchers.The % AC efficiency was 78 and 82 %, these values were relatively higher compared to the reported efficiency of 20.78% (Hameed et al 2009), 40% (Ahmad 2010), 51% (Sahu 2010). The moisture content of the SAC and SAT are 18.24% and 12.10% which are slightly higher than some reported values of 4.5% (Salman 2011), 9.8% (Mane 2005) and with SAT slightly lower than 13.2% (Ioannidou 2007). The SAC FTIR spectrum (Figure 1) showed a peaks at 3533.14, 3518.65, 3454.16, 1651.34, 1384.54,1158.25, and 561.96 cm^{-1}. The peak at 3533.14 and 3518.65 cm^{-1}. The peak at 3454.16 cm^{-1} indicate O-H stretching due to water, peaks at 1655.34 cm^{-1} and 1384.54cm^{-1} represent C=N and C=C stretching due to the aromatic ring in the secondary metabolites present and the peak at 1158.25 cm^{-1} is due to C-OH corner band symmetry stretching in the aromatic ring while those of 561.96 cm^{-1} indicates C-Br stretch due to alkyl halides. The results obtained are in agreement with the works reported by Preeti 2017; Flora *et al*., (2018). The SAT FTIR spectrum (Figure 2) shows peaks at3441.12, 2357.09, 1473.66, 1153.47, 675.11 and 597.95 $cm^{-1.}$ The peak at 3441.12 cm^{-1} represent O-H Stretching H-bonded due to alcohol/phenols. The absorption band 2357.09 cm^{-1} indicate C≡C triple bond stretching due to the alkynes terminal, 1473.66 cm^{-1} indicate aromatic –C-C stretching. The peak at 1153.47 cm^{-1} represent C-O bond stretching due to alcohol while 675.11 cm^{-1} is due to C-Br alkyl halides as reported by Kurek, *et al.,* 2021.

Table 1. Physico-chemical characterization, SEM, XRD and FTIR assignments

NPs	SAC	SAT
Yield (%)	78	82
Moisture (%)	18.24	12.10
XRD (nm)	29.57	26.55
SEM	Granular and partially spherical	Porous, granular and partially spherical
FTIR (cm^{-1})	3533 (OH), 1655 (CN), 1158 (COH), 561 (CBr)	3441(OH),1408 (C-C), 1153 (C-O), 673(CBr)

FTIR result

SAC and SAT FTIR result

The FTIR spectrumSAC is presented inFigure.1. It shows several peaks at 3533.14, 3518.65, 3454.16, 2383.94, 1651.34, 1384.54,1158.25, 941.18 and 561.96cm^{-1}. The peak at 3533.14 and 3518.65cm^{-1} represent O-H stretching due to the flavonoid. The absorption band at 3454.16cm^{-1} indicate O-H stretching due to water, peaks at 1655.34 cm^{-1} and 1384.54cm^{-1} represent C=N and C=C stretching due to the aromatic ring in the secondary metabolites present and the peak at 1158.25cm^{-1} is due to C-OH

corner band symmetry stretching in the aromatic ring while those of 941.18 cm^{-1} and 561.96 indicates C-Br stretch due to alkyl halides. The result obtained are in agreement with the literature reported by (Preeti, 2017) which shows that the FTIR bands obtained indicate the present of flavonoids, polyphenols, triterpenes and amide present in the *P.niruri*leaves extract and that of (flora *et al*., 2018). Which show that, the FTIR bands obtained are characteristics of flavonoids, triterpenes, furanoid, sugar, coumarins tannins, phenols and acid present in the acqeous extract of *propolis.*

For the SAT, the FTIR spectrum is depicted in Figure 2. The spectrum shows some prominent peaks at 3441.12, 2357.09, 1473.66,1153.47, 675.11 and 597.95 $cm^{-1.}$ The peak at 3441.12 cm^{-1} represents O-H Stretching H-bonded due to alcohol/phenols. The absorption band 2357.09 cm^{-1} indicate C≡C triple bond stretching due to the alkynes terminal, 1473.66 cm^{-1} indicate aromatic –C-C stretching. The peak at 1153.47 cm^{-1} represents C-O bond stretching due to alcohol while 675.11 cm^{-1} is due to C-Br alkyl halides (Kurek*et al.,* 2021).

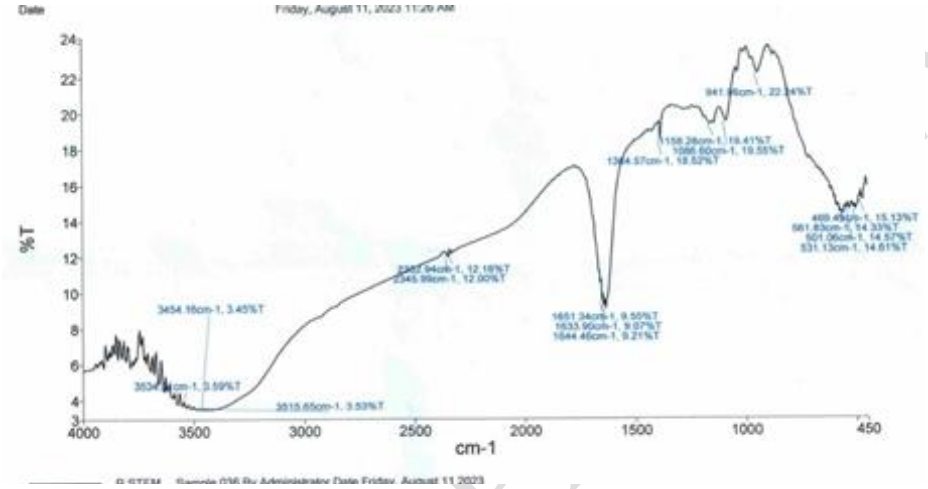

Figure 1 SAC FTIR spectrum

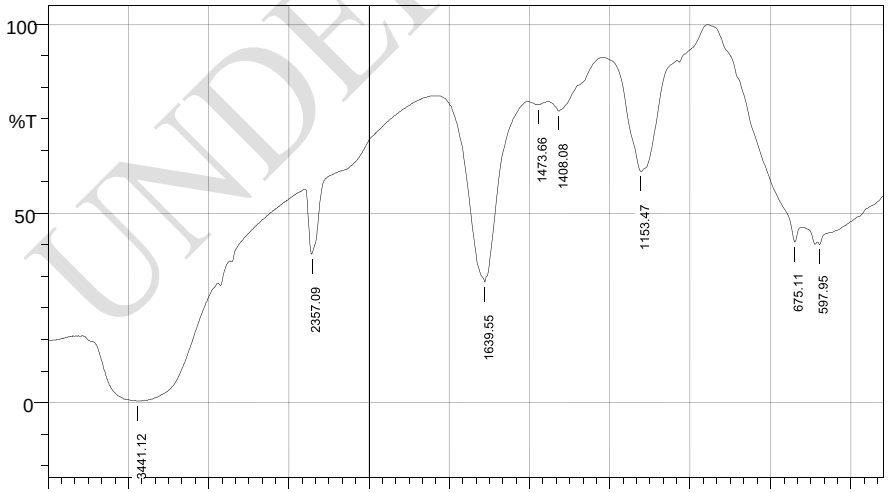

Figure2. SAT FTIR spectrum

SAC and SAT SEM result

The SEM image for SAC is presented in Figure 3. The image shows that the particles are porous like structure which are partially spherical, granular aggloramated in nature. The result obtained is in agreement with the work done by Sugumaran *et al.,* (2021).

The SEM image obtained for SAT is presented in Figure.4. The image shows that the particles are porous like structure which is partially spherical and granular in nature. The result obtained is nearly in agreement to the work done by (Sugumaran *et al.,* 2021) showed the porouslikemorphology when prepared and characterized activated carbon from the banana empty fruit bunch and *Delonix regia* fruit pod.

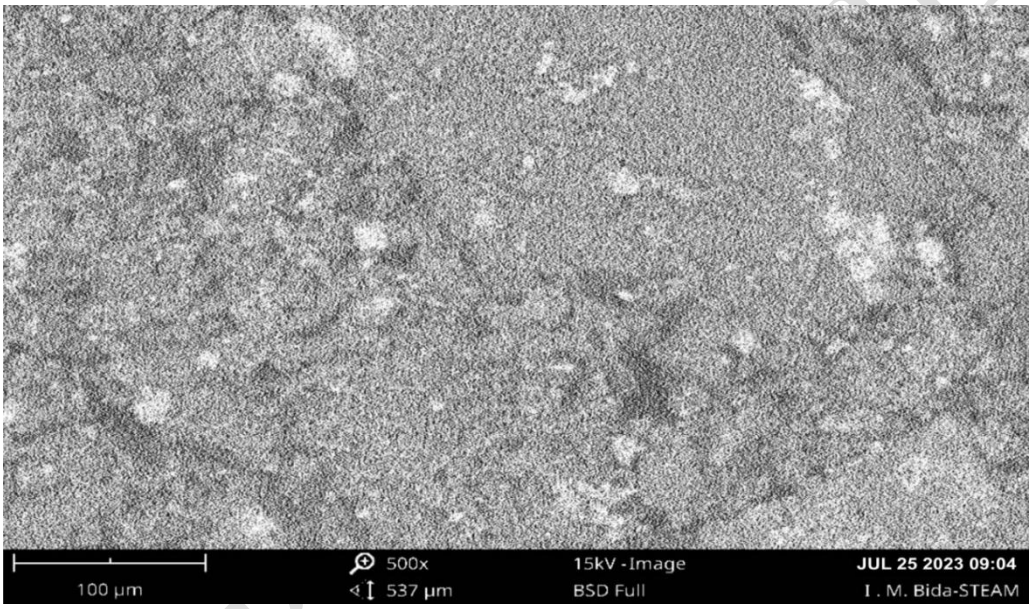

Figure.3. SEM image for SAC

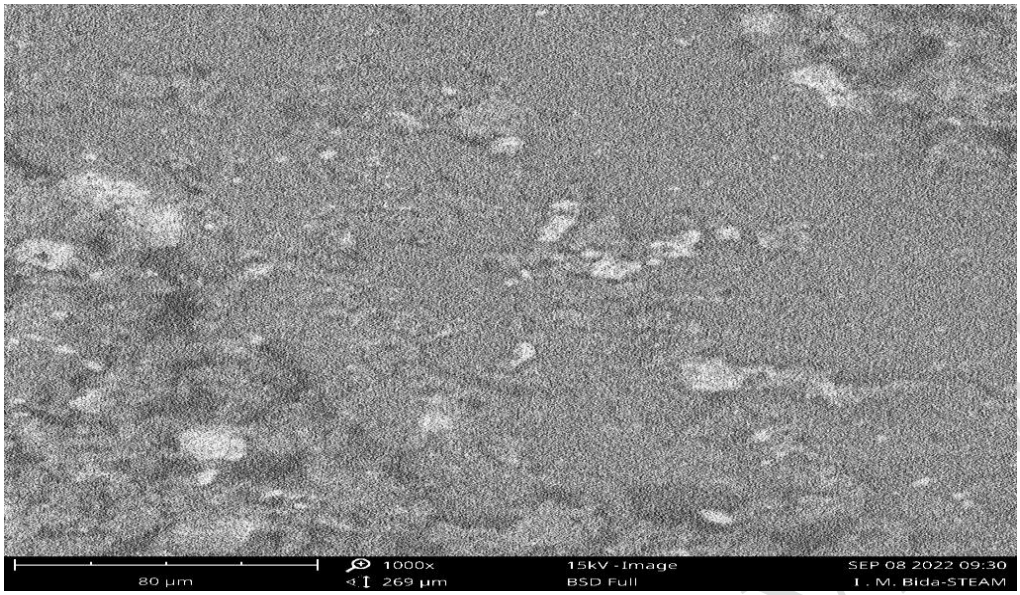

Figure .4. SEM image for SAT

SAC SAT XRD result

The XRD pattern of SAC is shown in Figure 5. The diffraction peaks were found at 2Θ = 27.46^0, 29.28^0, 34.57^0 and 56.39^0, with respect to the plane of (101), (200), (211) and (311). It also shows Face Centered Cubic (FCC) structure and the average crystalline size of 29.57nm. For the SAT, the XRD chromatogramis depicted in Figure.6. The peaks were found at 2Θ = 25.36^0, 26.29^0, 30.17^0 and 54.37^0, with respect to the plane of (101), (200), (211) and (311). It shows Face Centered Cubic (FCC) structure and the average crystalline size of 26.55nm, this corresponds to the work done by (Padilla *et al.,* 2021).

These Bragg's peaks might have been resulted from bioorganic compounds present in the black currant stem. Summary of the characterization results is shown in Table 1. SAT was chosen based on the particle size obtained from the XRD analysis.

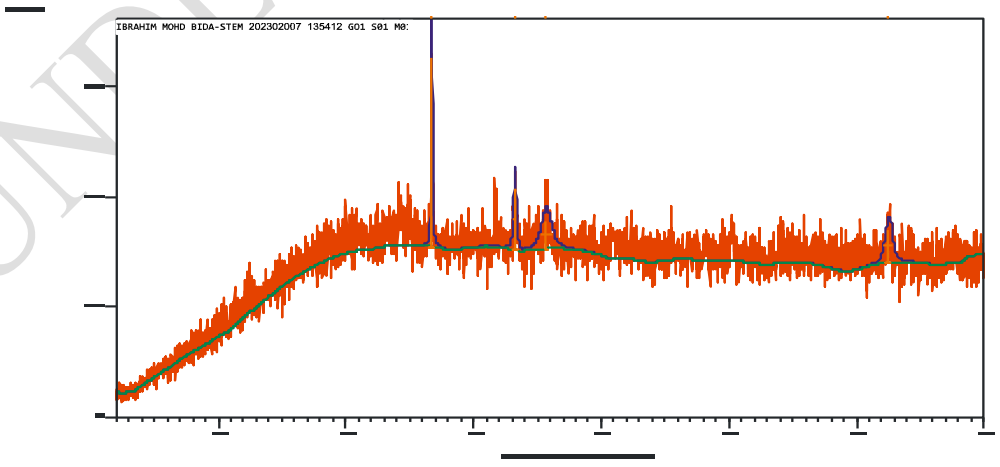

Figure 5. SAC XRD chromatogram

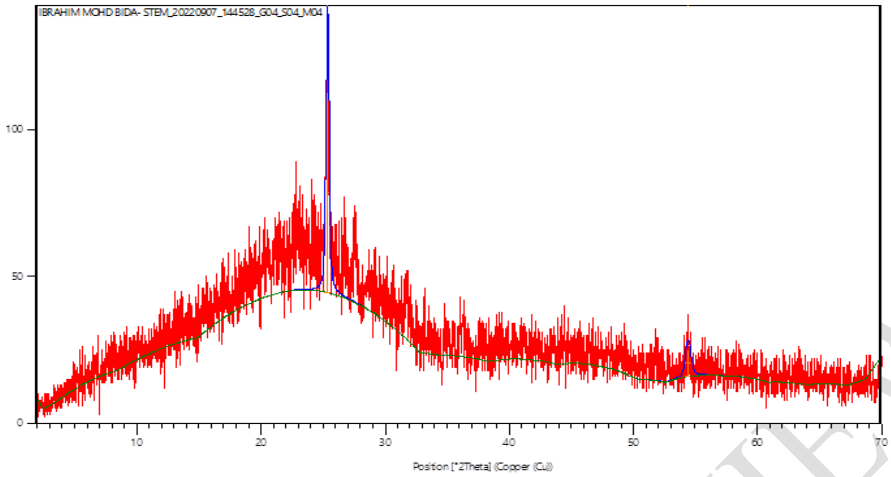

Figure.6 Shows XRD image of SAT

Adsorption studies

Effect of Initial Concentration

The effect of initial metal (Pb^{2+}) ion concentration (50 – 250 mg/L) on SAT is presented in Figure 7. The adsorbent dose (0.5 g), pH (7), shaking time (30 min) and temperature (298 K) were kept constant. From the results obtained, percentage removal of lead (ii) ion (Pb^{2+}) on SAT (Pb-SAT) slightly decreased with increase in initial concentration. At low initial concentrations (50 mg/L) most of the metal ions were removed/adsorbed from the aqueous solution. The slight decreased in uptake at low initial metal ion concentration could be attributed to unavailability of vacant sites on the SAT for metal binding (Pindiga*et al*., 2022)

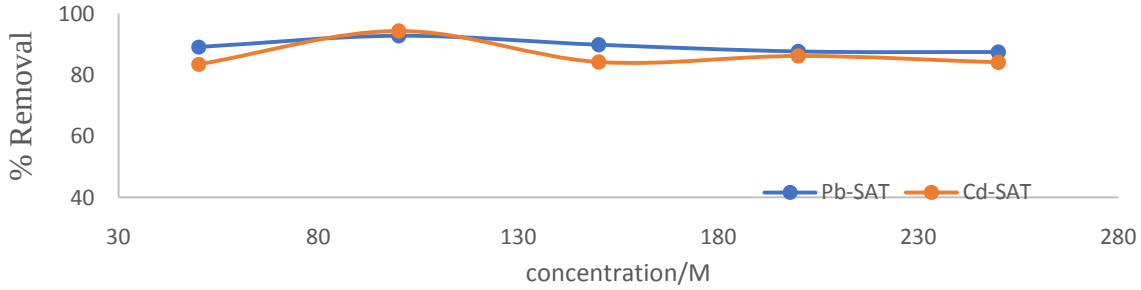

Figure 7. Effect of initial metal concentration on SAT

Effect of adsorbent dosage

A dosage study is an important parameter in adsorption studies because it determines the capacity of adsorbent for a given initial concentration of metal ion solution. The effect of adsorbent dose (SAT) on the percent removal of $Pb^{2+}$and $Cd^{2+}$was studied with varying dosage of 0.2, 0.4, 0.6, 0.8, and 1 g while, concentration (50 mg/L), pH (7), shaking time (30 min) and temperature (298 K) were constant. From Figure 8, it can be observed that increased in adsorbent dose of SAT increase the %removal of $Pb^{2+}$and

$Cd^{2+}$from 92.78 and 94.38%. Beyond the optimum dose the removal efficiency slight decreased to 89.84 and 84.25% for the SAT respectively. As expected, the removal efficiency increased with increase in adsorbent dose because for a fixed initial adsorbate concentration, increasing adsorbent dose provides more adsorption sites (Mousavi*et al.,*2010).Thus,0.8 g of the nanoparticles was used throughout the study.

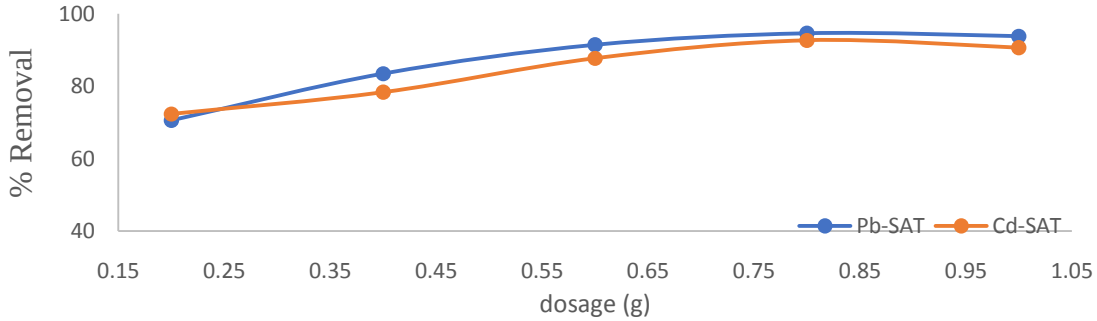

Figure .8. Effect of adsorbent dose on SAT for removal of Pb^{2+} and Cd^{2+}

Effect of time

The effect of time on the adsorption rate of Pb^{2+} by SAT was carried out at different time interval (10, 20, 30, 40 and 60 min) while, other parameters were kept constant. The removal of aqueous $Pb^{2+}$and Cd^{2+} by SAT increased with increase in time with optimum uptake of 92.49% and 90.25% at 40 min for the Sat respectively. The results of the effect of time on $Pb^{2+}$and Cd^{2+} removal by SAT is presented in Figure9. The results are in agreement with the work reported by Abdel-Ghani *et al.,*2007.

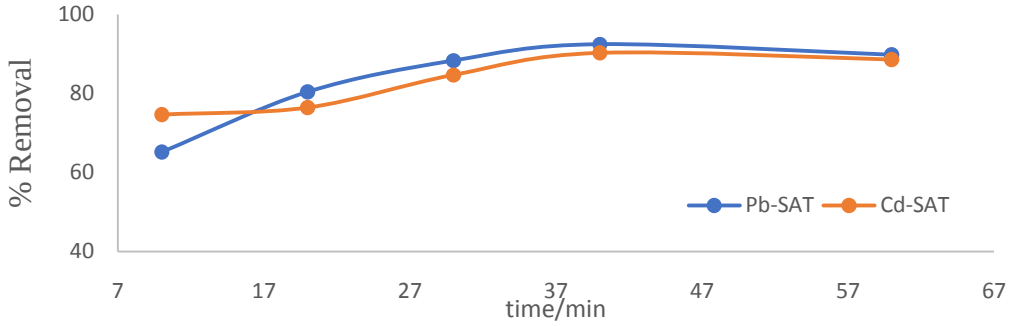

Figure .9. Effect of time on SAT for removal of Pb^{2+} and Cd^{2+}

Effect of temperature

Effect of temperature was studied by conducting the experiment at different temperatures of 298, 303, 308, 313 and 333 K while, other parameters were kept constant. As presented in Figure .10, the %removal of Pb^{2+} and Cd^{2+} increases with increased in temperature with optimum uptake of 90.95 and 88.26% at 308 K for the SAT respectively. This may be due to the endothermic nature of the adsorption process (Pindiga*et al.,*2022).

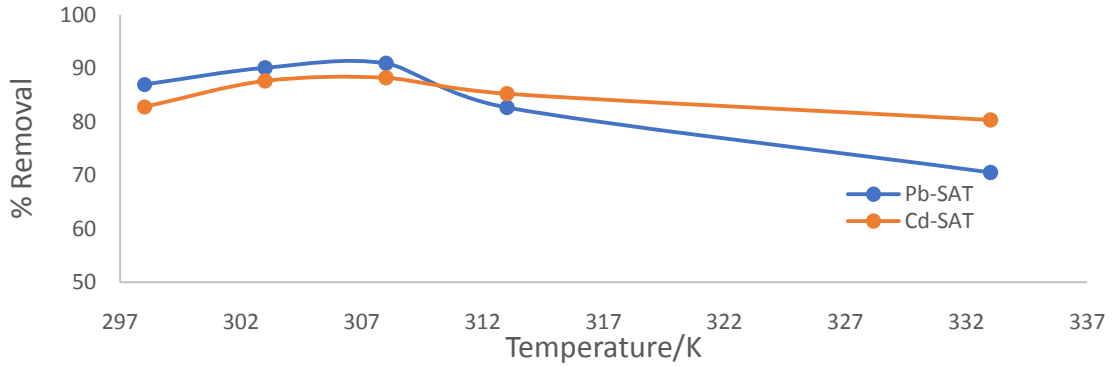

Figure 10. Effect of temperature on SAT for removal of Pb^{2+} and Cd^{2+}

Effect of pH

pH is one of the important controlling parameters in adsorption of process. The effect of pH on $Pb^{2+}$and Cd^{2+} uptake by SAT is shown in Figure 11 It is evident from the result, that the highest percentage (>70%) of Pb^{2+} removal was found at pH 7 for theSAT. This could be attributed to the fact that the concentration of H_3O^+ ion was high at low pH and it will cause competition between H_3O^+ and metal ions for active sites on the surface of the biosorbents (Pindiga, *et al.,* 2022**).**

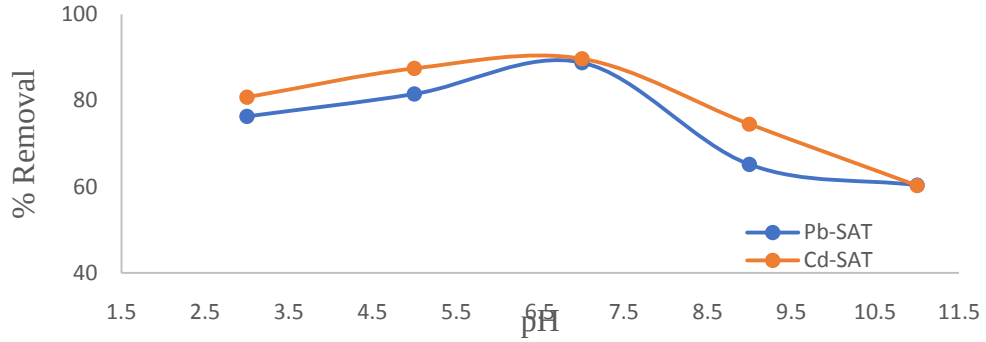

Figure .11. Effect of pH on SAT for removal of Pb^{2+} and Cd^{2+}

Adsorption isotherm

An adsorption isotherm represents an equilibrium relationship between the adsorbate concentration in the liquid phase and that on the adsorbent surface at a given condition. In the present study Langmuir and Freundlich models were used to described the equilibrium data. These data fitted well into Langmuir and Freundlich models (Figures.12). The test of data indicated that the adsorption of Pb^{2+} and Cd^{2+} on SAT are best described by Langmuir and Freundlich adsorption isotherms. The separation parameters K_L is an indication of level of interaction between the adsorbate and adsorbent (Abdul-Salam and Magaji, 2016). The adsorption of a molecule onto adsorbent may be described as favorable ($K_L > 1$), linear ($K_L = 1$) favorable ($0 < K_L < 1$) or irreversible ($K_L < 0$) based on the calculated K_L value. The K_L in the metals (Pb^{2+} and Cd^{2+}) are less than unity indicating that the adsorption process was favorable. Therefore, SAT is excellent adsorbents for the uptake of Pb^{2+} and $Cd^{2+}$the isothermal constant and regression coefficients are summarized in Table 2.

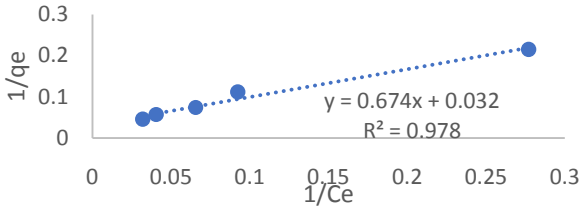

Figure 12. A graph of Langmuir isotherm for Pb^{2+} on SAT

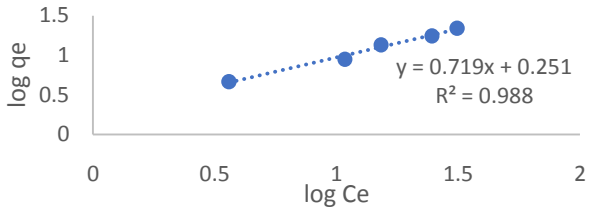

Figure 13. A graph of Freundlich isotherm for Pb^{2+} on SAT

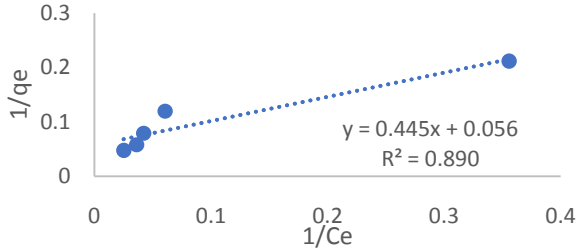

Figure 14. A graph of Langmuir for Cd^{2+} on SAT

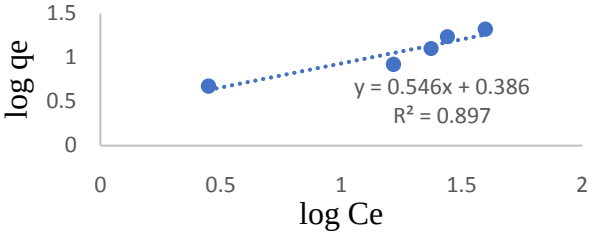

Figure.15. A graph of Freundlich for Cd^{2+} on SAT

Adsorption kinetic study

The data obtained from the influence of time on the adsorption of Pb^{2+} and Cd^{2+} onto SAT were subjected to the pseudo-first order and pseudo-second order kinetics equations for a test for a test of fitness of data and the plots are presented in Figures 16. It was found that all the data fitted into the pseudo-first and pseudo-second order models. The linearity of the plots with R^2 values that are close to unity indicates that the adsorption process followed pseudo-second order better than pseudo-first order model. A number of adsorption process have been reported to fit well into second order kinetic model (Abdul-Salam and Magaji, 2016; Abdul-Salam and Magaji 2014). Table 3 summarizes the kinetics parameters for pseudo-first and pseudo-second order models.

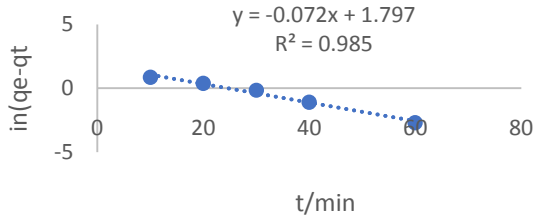

Figure 16.Plot of Pseudo-first order kinetics for Pb^{2+}on SAT

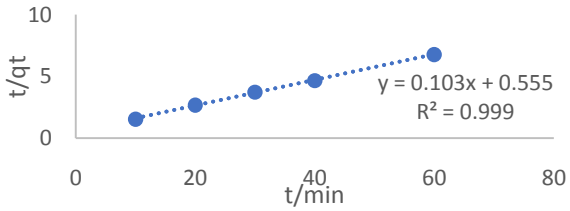

Figure 17. Plot of Pseudo-second order kinetics for Pb^{2+}on SAT

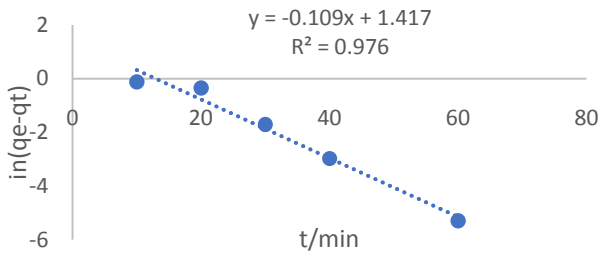

Figure 18. Plot of Pseudo-first order kinetics for Cd^{2+} on SAT

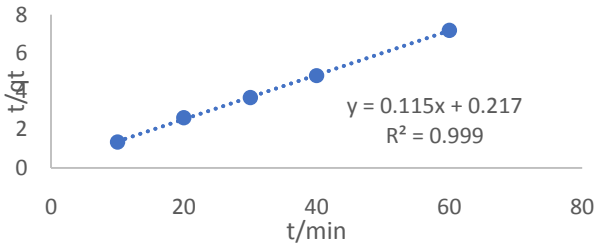

Figure 19. Plot of Pseudo-second order kinetics for Cd^{2+} on SAT

Table 2. Isotherms and kinetics parameters of adsorption of Pb^{2+} and Cd^{2+}

Isotherm Model	**Metal ion**	
	Pb^{2+}	**Cd^{2+}**
Langmuir		
q_m(mg/g)	30.8642	17.574
K_L (L/g)	0.0480	0.127
R^2	0.9789	0.890
Freundlich		
K_F (mg/g)	1.78361	2.43725
n	0.7192	0.5465
R^2	0.9886	0.8976
Pseudo-first-order		
qe_{cal}	6.031	0.777
K_1	0.073	-1.417
R^2	0.985	0.9767
Pseudo-second order		
qe_{cal}	9.625	8.628
K_2	0.019	4.606
R^2	0.999	0.995

Adsorption thermodynamics

This study gives general information about the influence of temperature on the adsorption and particularly useful to predict the feasibility of the adsorption process. The standard free energy (ΔG), the enthalpy (ΔH) and the entropy (ΔS) were calculated from the Gibb's free energy and Van't Hoff equations 4 ton 7 (Abdul-Salam and Magaji, 2014).

$$K = \frac{C_{Ae}}{C_e} \quad (4)$$

$$\Delta G = -RT\ln K \quad (5)$$

$$InK = \frac{\Delta S}{R} - \frac{\Delta H}{RT} \quad (6)$$

$$\Delta G = \Delta H - T\Delta S \quad (7)$$

Where C_e is the equilibrium concentration in solution (mg/L) and C_{Ae} is the equilibrium concentration on the sorbent (mg/L) and K is the equilibrium constant. The thermodynamic parameters are presented on Table 3.

The values of ΔH and ΔS were obtained from the slope and intercept of Van Hoff's plot of InK versus 1/T. The negativity of ΔG reflects the feasibility of the adsorption process for Pb^{2+} and Cd^{2+}. Generally, ΔG for physisorption processes ranges from 0 and 20 kJ/mol while, the chemisorption's is between -80 and 400 kJ/mol (Sen *et al*., 2011; Abdul-Salam and Magaji, 2016). Therefore, the uptake of Pb^{2+} and Cd^{2+} by SAT is physisorption process. The type of a sorption process can be explained in terms of the magnitude of ΔH. Generally, the ΔH values for physisorption and chemisorption are within the range of 2.1 – 20.9 kJ/mol and 80 – 200 kJ/mol respectively (Absul-Salam and Magaji, 2016).

The positivity and the magnitude of ΔH values obtained for the adsorption of Pb^{2+} and Cd^{2+} suggest an endothermic and physisorption process (Table 3) for SAT on Pb^{2+} and Cd^{2+}. The positive values of ΔS revealed that there were increased in randomness at the aqueous-SAT interface during the metal's uptake.

Table 3. Thermodynamics parameters for uptake of Pb^{2+} and Cd^{2+} on SAT

Temperature (K)	**ΔG° (KJ mol^{-1})**	
	Pb^{2+}	Cd^{2+}
298	-1.443	-0.339
303	-1.117	-0.513
308	-0.833	-0.859
313	-0.616	-1.546
333	-0.060	-2.433
ΔH° (kJ mol^{-1})		
	+12.754	+18.377

ΔS°(J mol-1 K^{-1})		
	+41.805	+12.151

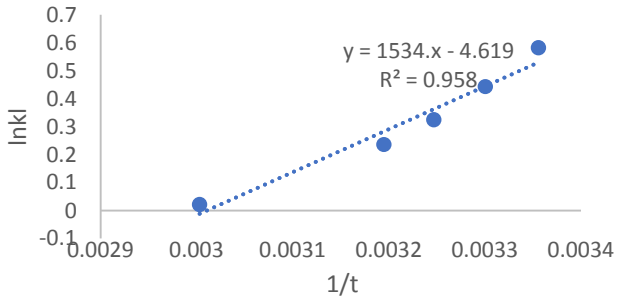

Figure 20 showing thermodynamic graph for Pb^{2+}on SAT

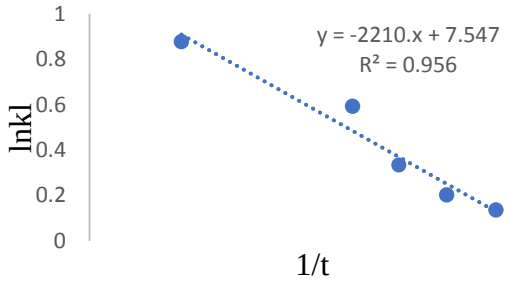

Figure 21 showing thermodynamic graph for Cd^{2+}on SAT

Conclusion

The preparation of SAC and SAT from the stem of black current was achieved through single and double-steps process of carbonization and activation. The performance was evaluated through batch equilibration of Pb^{2+} and Cd^{2+} ion for the purpose of optimization of adsorbent dose, metals concentration and temperature conditions. The uptake increased with increasing agitation time, concentration and temperature. The adsorption equilibrium was attained in 60 min of agitation time. The kinetic data obtained from this study showed good correlation coefficient for a pseudo-second order kinetic model. The equilibrium data conformed well into the Freundlich isotherm than Langmuir with a high correlation coefficient close to unity, indicating that the adsorption of the metal ion solutions onto surface of SAT followed a multilayer pattern. Thermodynamic quantities such as Gibbs free energy (ΔG), the enthalpy (ΔH) and the entropy change of sorption (ΔS) were evaluated and indicated that the adsorption process was spontaneous and endothermic. Therefore, SAT could be considered as alternative biomass for the removal of single metal solution of Pb^{2+} and Cd^{2+} since it was found to be effective, low cost, abundant and can be source locally.

References

Abdel-Ghani, N.T., Hefny M., El-Chaghaby G.A.F. (2007). Removal of lead from aqueous solution using low cost abundantly available adsorbents. *Internation. Journal. Environmental Science Techenology*. 4(1): 67-73.

Abdus-Salam N., and Magaji B. (2016). Adsorption of Alizarin and Fluorescein Dyes onto Palm Seeds Activated Carbon Kinetic and Thermodynamic Studies. *Journal Chemistry* Society Pak**,** 38, 04.

Abdus-Salam, N., and Magaji., B. (2014). Adsorption of alizarin and fluorescein dyes onto palm seeds activated carbon: Kinetic and thermodynamic studies *Journal of Science and Technology,* 15, 1.

Ahamed, A.J., and Shajudha A.B. (2012). Adsortion of copper from aqueous solution using low cost adsorbent; achieves of applied science research. 1532 –1539.

Flora., P., Darshin, S.K., and Jone., T. (2018). Green synthesis of silver nanopsiticles from propolis. Research. *Journal of Life Science, Bio in Formatics, Pharmaceutical and Chemical Sciences*, 23 - 36.

Kurek, M., Benbettaieb, N., Scetar, M., Chaudy, E., Repajic, M., Klepac, D., Valic, S. Debeaufort, F., Galic, K. (2021). Characterization of Food Packaging Films with Blackcurrant Fruit Waste as a Source of Antioxidant and Color Sensing Intelligent 26, 25-69.

Mousavi H.Z., Hosseynifar A., Jahed V., and Dehghani S.A.M. (2010). Removal Of Lead From Aqueous Solution Using Waste Tire Rubber Ash As An Adsorbent. *Brazilian Journal of Chemical Engineering,* ISSN 0104-6632.

Padilla‐ Cruz A.L, Garza‐ Cervantes J.A., Vasto‐ Anzaldo X.G., Gerardo García‐ Rivas, A. León‐ Buitimea and Morones‐ Ramírez J.R. (2021). Synthesis and design of Ag–Fe bimetallic nanoparticles as antimicrobial Synergistic Combination therapies against clinically relevant pathogens Scientific report, 11(2921): 1-14

Sugumaran, P., Susan, V., Ravichandran and Seshadri, S., (2012). Projuction and Characterization of Activated Carbon from Banana Empty Fruit Bunch and Delonix Regia Fruit Pod. *Journal of Sustainable energy and environment,***3**, 125 – 132.

Paul, B.T., Clement G.Y., Anita K.P., and Dwayne J.S. (2014). Heavy Metals Toxicity and the Environment, National Institute of Health Public Access Author Manuscript, 101, 133–164.

Pindiga, N.Y., Walid A.H., Abdullateef, O.A., and Mohammad, A.B. (2022). Kinetic, Equilibrium and Thermodynamic Study of the Adsorption of Pb (II) and Cd (II) Ions from Aqueous Solution by the Leaves Biomass of Guava and Cashew Plants. *Online Journal* of Chemistry, 2(1): 23–38.

Sivaraj, R., & Rajendran, V. (2010). Preparation and Characterization of Activated Carbons from Parthenium Biomass by Physical and Chemical activation techniques, *Journal of chemistry*. 7(4): 1314-1319.